*Molecular Vision* 2019; 25:70-78 <http://www.molvis.org/molvis/v25/70>
Received 4 August 2018 | Accepted 5 February 2019 | Published 7 February 2019



# Comparison of histologic findings in age-related macular degeneration with RPE flatmount images

**Qing Zhang,[1] Micah A. Chrenek,[1] Shagun Bhatia,[1] Alia Rashid,[1] Salma Ferdous,[1] Kevin J. Donaldson,[1] Henry Skelton,[1] Wenfei Wu,[1] Thonnie Rose O. See,[1] Yi Jiang,[2] Nupur Dalal,[1] John M. Nickerson,[1] Hans E. Grossniklaus[1,3]**

*[1]Department of Ophthalmology, Emory University School of Medicine, Atlanta, GA; [2]Department of Mathematics and Statistics, Georgia State University, Atlanta, GA; [3]Department of Pathology, Emory University School of Medicine, Atlanta, GA*

**Purpose:** To visualize and analyze ex vivo flatmounted human RPE morphology from patients with age-related macular degeneration (AMD), and to compare the morphology with histologic findings. To establish whether the sub-RPE structures identified en face in RPE flatmount preparations are drusen with histopathological registration in serial sections. To detect characteristic patterns found en face in RPE with the same structures in histological cross sections from eyes from cadavers of patients with AMD.

**Methods:** Twenty-eight postmortem eyes from 14 patients (16 eyes with AMD and 12 age-matched control eyes) were oriented and microdissected yielding a RPE-choroid preparation. The tissues were flatmounted, stained with Alexa Fluor 635 Phalloidin (AF635-phalloidin) for f-actin and propidium iodide for DNA, and imaged using confocal microscopy. Portions of tissue from macular regions were processed for electron microscopic examination. After confocal imaging, the samples were remounted for histologic processing, embedded in paraffin, and serially sectioned perpendicular to the plane of the RPE-choroid sheet. Scaled two-dimensional (2D) maps of drusen locations found with the histological cross sections were constructed and correlated with the en face confocal microscopic images.

**Results:** Twenty-eight postmortem eyes with a mean time of death to tissue preservation of 23.7 h (range 8.0–51 h) from 14 donors (seven women and seven men) with an average age of 78 years (range 60–93 years) were evaluated. Eight donors had AMD, and six served as controls. Scattered small, hard drusen were present in the periphery of the eyes with AMD and the healthy eyes. The macular region of the eyes with AMD contained small (<63 µm), medium (63.0–124 µm), and large (125 µm) drusen. The RPE was arranged in rosette-like structures overlying small drusen, attenuated overlying medium-sized drusen, and consisted of large multinucleated cells overlying large drusen. The RPE in the area of geographic atrophy was attenuated and depigmented.

**Conclusions:** Confocal images of flatmounts from eyes with AMD showed RPE patterns overlying various types of drusen and geographic atrophy that correlated with histologic characteristics. We propose RPE repair mechanisms that may result in the patterns that we observed.

Age-related macular degeneration (AMD) is the leading cause of visual loss among persons 65 years old and older in industrialized countries [1-4]. Despite basic and clinical research, the pathogenesis of AMD remains unclear, likely due to the multifactorial nature of the disease. There appear to be complex interactions of metabolic, functional, genetic and environmental factors in AMD which result in structural changes in the macula, including photoreceptor, retinal pigment epithelium (RPE), Bruch's membrane and choriocapillaris changes [5].

The RPE is a monolayer of hexagonal cells that forms the barrier between the choriocapillaris and neurosensory retina in the normal human eye. It has many physiological functions, including maintenance of the blood outer retinal barrier, regulation of ion balance, participation in the visual cycle, expression of growth factors, and phagocytic uptake and degradation of shed photoreceptor outer segments [5-8]. Throughout life, RPE cells accumulate lipofuscin, which results from incompletely degraded proteins or phagocytized photoreceptor membranes. RPE morphologic changes in AMD progression may occur secondary to cellular kinetics, metabolism, or damage [3,4,9-11]. However, the relationship between RPE morphometry in AMD and "normal" cell death that occurs in aging is unclear [12]. In this study, we determined in micro scale within the bounds of the excised specimens the topographic patterns of human RPE cells in AMD eyes compared with age-matched control eyes. Age related RPE changes in human AMD eyes were analyzed using an in situ RPE flatmounts and correlated these findings with the pathologic findings in 2-dimensional (2D) histologic mappings. We found RPE morphometric patterns

Correspondence to: Hans E. Grossniklaus MD, L.F. Montgomery Ophthalmic Pathology Laboratory, BT428, 1365 Clifton Road, Atlanta, GA 30322; Phone: (404) 778-4611; FAX: (404) 778-2231; email: ophtheg@emory.edu

Table 1. Donor information.

| Case | Age (years) | Sex | Race | Diagnosis | Hours 1 | Hours 2 |
|---|---|---|---|---|---|---|
| 1 | 86 | M | C | AMD | 5 | 33 |
| 2 | 89 | F | C | AMD | 4 | 24 |
| 3 | 76 | F | AA | AMD | 8 | 23 |
| 4 | 77 | M | C | AMD | 7 | 8 |
| 5 | 93 | F | C | AMD | 6 | 15 |
| 6 | 81 | F | C | AMD | 20 | 24 |
| 7 | 72 | M | C | AMD | 11 | 25 |
| 8 | 75 | F | C | AMD | 6 | 15 |
| 9 | 87 | F | C | normal | 4 | 13 |
| 10 | 82 | M | C | normal | 15 | 30 |
| 11 | 60 | M | AA | normal | 4 | 20 |
| 12 | 70 | F | C | normal | 9 | 23 |
| 13 | 71 | M | C | normal | 7 | 51 |
| 14 | 75 | M | C | normal | 4 | 28 |

Abbreviation: M=male, F=female, C=Caucasian, AA= African American, AMD=age related macular degeneration; Hours 1=time from death to enucleation; Hours 2=time from death to preservation.

that are associated with underlying small, intermediate, and large drusen and basal laminar deposit. We propose various mechanisms of RPE injury and death that may result in these patterns.

## METHODS

*Tissue acquisition:* The study protocol adhered to the tenets of the Declaration of Helsinki for research involving human subjects and Association for Research in Vision and Ophthalmology (ARVO) guidance for human tissue. This study was approved by the Emory University Institutional Review Board (IRB). Twenty-eight human postmortem eyes (16 non-exudative AMD and 12 age-matched control eyes) were obtained from the North Carolina Eye Bank, within 48 hours of death and stored in moist chambers at 4 °C after enucleation. The AMD eyes were identified from donors who had histories of non-exudative AMD as listed in Table 1. “Control” eyes were obtained from donors with no known history of any eye disease except cataract surgery (e.g., we excluded AMD, diabetic retinopathy, or glaucoma). The age of donors ranged from 60 to 93 years. The cornea, iris and lens were removed from the enucleated eyes (Figure 1A) and fixed in 10% buffered formalin (pH 7.4) for 4 hours subsequently it was stored in phosphate buffered saline (PBS), 1X; 155.17 mM NaCl, 2.97 mM $Na_2HPO_4$-$7H_2O$, 1.06 mM $KH_2PO_4$, pH 7.4 (PBS, Product number 10010023, ThermoFisher Scientific, Carlsbad, CA) at 4 °C. The time interval between death and preservation ranged from 8 to 51 h and averaged 23.7 h. Eyes were grossly examined and photographed with Olympus microdissection microscope (DP20, Olympus, Tokyo, Japan).

*RPE flatmount tissue processing:* RPE flatmounts were prepared using a microdissection technique as follows. Briefly, eyes with corneal cap removed were placed under a dissecting microscope and the macula was identified. (Figure 1B). Six radial anterior-posterior oriented scleral cuts were placed at the ora serrata and extended towards the optic nerve to enable the tissue to be flattened. (Figure 1C). Residual scleral and limbal tissue was trimmed. A star-shaped flatmount was placed on a glass slide. The scleral petals were carefully peeled away with a fresh scalpel blade to expose the intraocular tissue with attention paid in the areas of vortex veins and fovea (Figure 1D). The retina and vitreous were subsequently removed in one piece by gently teasing away the RPE-choroid sheet from the ciliary insertion with the specimen submerged in PBS buffer. (Figure 1E) The flatmount preparation was divided into six portions (temporal, inferotemporal, inferonasal, nasal, superonasal, and superotemporal) and 4x4mm peripheral retinal samples from each petal approximately 10 mm away from the fovea and the macula were separated and prepared for staining and confocal imaging (Figure 1F).

*Staining and Confocal Imaging:* After dissection, the tissues were flatmounted, RPE side up, onto conventional microscope slides to which a silicon gasket had been applied (Grace Bio-Labs, Bend, OR). The specimens were rinsed with PBS followed by incubation with 2.5% AF635-phalloidin

(Invitrogen, Camarillo, CA) and 20 µg/ml propidium iodide (ThermoFisher Scientific) in 0.1% Triton X-100 HBSS solution overnight at room temperature. Subsequently, the specimens were washed 3 times with 0.1% Triton X-100 in HBSS buffer, mounted with 2 drops vectashield hardset (Vector Labs, Burlingame, CA), coverslipped, and allowed to set overnight. The slides were stored up to 1 month in the dark at 4 °C until evaluation using a Nikon Ti inverted microscope with C1 confocal scanner. Using an automated XY stage control within the EZ-C1 software, the flatmount was imaged with a 20x objective lens (numerical aperture = 0.75) (Nikon Instruments Inc., Melville, NY). Autofluorescence was excited using the argon gas 488 nm laser and emissions were pseudo colored with blue. AF635-phalloidin was excited using 638 nm solid state laser and emission was pseudo colored with green. Propidium iodide was excited with 561 nm DPSS laser pseudo colored with red. Image were processed as described from previous study [13]. Briefly, confocal images from the entire flatmount were photomerged using Photoshop CS2 (Adobe Inc., San Jose, CA) and zoning layers were applied. Extracted cutboxes from Photoshop CS5 were run and analyzed through CellProfiler Version 2.1 [14].

*Histological examination and 2D reconstructions:* Two-dimensional (2D) mappings of two representative AMD cases (cases 1 and 2) were reconstructed. Confocal scanning microscopy was done, specimens were placed in glass slides and incubated in a humidified container overnight at 4 °C. The specimens were gently removed from the glass slide, cut tissue sections were placed onto a filter paper with their orientation marked; it was dehydrated in increasing concentrations of alcohol, cleared in xylene and embedded in paraffin 90 degrees to the plane of the RPE-choroid sheet using Tissue-Tek® VIP® 6 (Sakura Seiki Co., Ltd. Nagano Japan). Serial 8 µm thick sections were prepared using a microtome (Shandon Finesse ME, Thermo Scientific, Astmore, UK) numbered in order, and stained with hematoxylin-eosin or periodic acid Schiff (PAS). The slides were sequentially examined under a microscope (Olympus BH-2, Olympus, Tokyo) and histologic findings of RPE changes, BlamD, and drusens were mapped and recorded using a standard reticule according to its orientation [4]. Six cases were examined by transmission electron microscopy (TEM). For TEM, a 2X2 mm representative portion of the specimen was fixed in 2.5% glutaraldehyde and post-fixed in 0.1 M cacodylate buffer and 1% osmium tetroxide. The specimens were then dehydrated, embedded in epoxy resin, and 1.0 µm thick sections were cut and stained with toluidine blue. Ultrathin sections (silver-gray ~30-60 nm thick [15]; were obtained and stained with uranyl acetate and lead citrate and examined by a transmission electron microscope (JEOL 100CX II, JEOL Ltd. Tokyo) with an image magnification of 4,800 to 5,800 X and recorded with electron microscope film (KODAK EM FILM 4489 size: 3 ¼" x 4", Eastman Kodak, Rochester, New York).

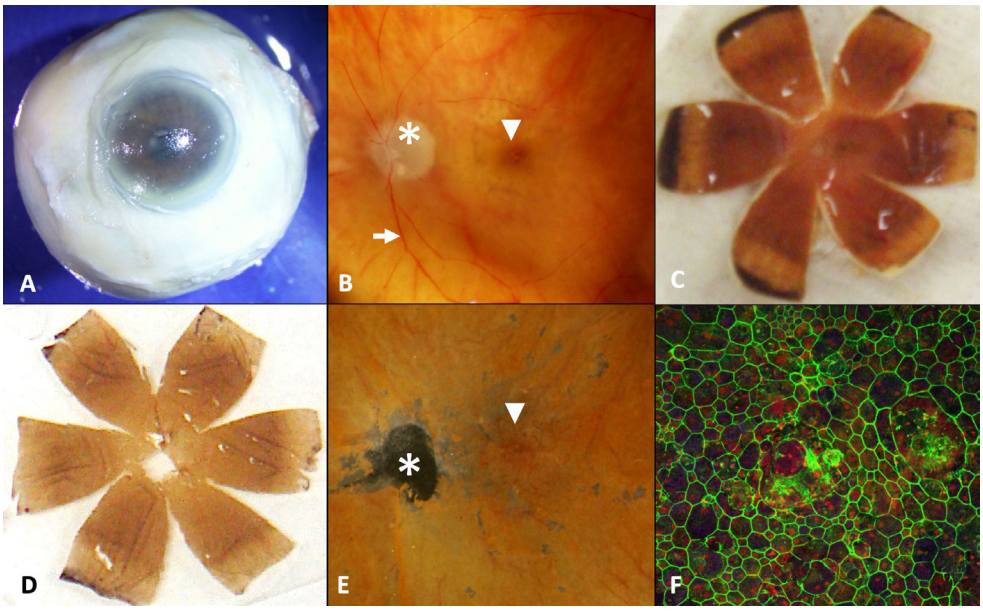


Figure 1. Retinal pigment epithelium (RPE) flatmount preparation. **A**: Post-mortem eye is grossly inspected. **B**: The eye is opened coronally and the anterior portion of the eye is removed, thus leaving a posterior optic nerve (asterix), sclera, choroid, RPE, retina including the macula (arrowhead) with the retinal vessels (arrow) and vitreous preparation. **C**: The posterior preparation is microdissected into six radial anterior-posterior petals. **D**: The sclera is removed from the petals leaving a retina, RPE, choroid preparation. **E**: The retina and vitreous are removed, thus leaving an RPE, Bruch's membrane, choroid preparation; macula (arrowhead); optic nerve defect (asterix). **F**: The RPE was stained with AF635-phalloidin pseudo colored with green and examined by confocal microscopy, thus yielding an RPE mosaic. This method of preparation is similar to that which we previously reported [13].

## RESULTS

*Donor information:* Twenty-eight human eyes were obtained from 14 donors (7 females, 7 males) with an average age of 78.1 years (range: 60-93 years). Donor ophthalmic history were requested from Georgia Eye Bank and reviewed. Eight donors (16 eyes) had AMD and six donors (12 eyes) served as controls. All patients with AMD had a history of non-exudative (dry) AMD. The time from death to enucleation (refrigeration) ranged from 4-20 h with a mean of 7.9 h, and the death to fixation (formaldehyde) time ranged from 8-51 h with a mean of 23.7 h. The causes of death included cardiac arrest, breast cancer, lung cancer, and colon cancer.

*Gross examination:* Gross examination showed that the cornea, sclera, anterior chamber, iris, and ciliary body were normal in all eyes. The lens was cataractous in 11 eyes. Posterior chamber intraocular lenses (PCIOLs) with lens remnants were present in 6 eyes, and the vitreous was posteriorly detached in 5 eyes. Pigmentary changes and small (<63 µm), intermediate (63-124 µm) and large (≥125 µm) drusen were observed in both macula and periphery in all AMD cases; whereas small drusen were present in both the macula and mid-periphery in two control eyes.

*Confocal microscopic examination of RPE-choroid sheet flatmounts:* Confocal microscopic examination showed many structures that were suspected to be large and diffuse soft drusen, defects in the RPE-choroid sheet, and irregularly-shaped RPE cells with multiple nuclei in the macular region of AMD eyes. In some areas, rosette-like structures were present, where RPE cells appeared to have filled in a defect. Representative images of tissue preparation and confocal imaging of the RPE are shown in Figure 2A-D. These findings and tentative identifications were tested by histological examinations of the corresponding light and electron microscopic features, and 2D histologic reconstructions, which allowed us to identify these structures in the en face RPE flatmounts conclusively after proper registration.

*Histologic examination and correlation with 2D histologic reconstructions:* Light microscopic examination showed that in all AMD eyes, hard and/or soft drusen were present in the macula. Representative images; small (Figure 3A-D), medium (Figure 3E-H), large (Figure 3I-L), soft drusen, and

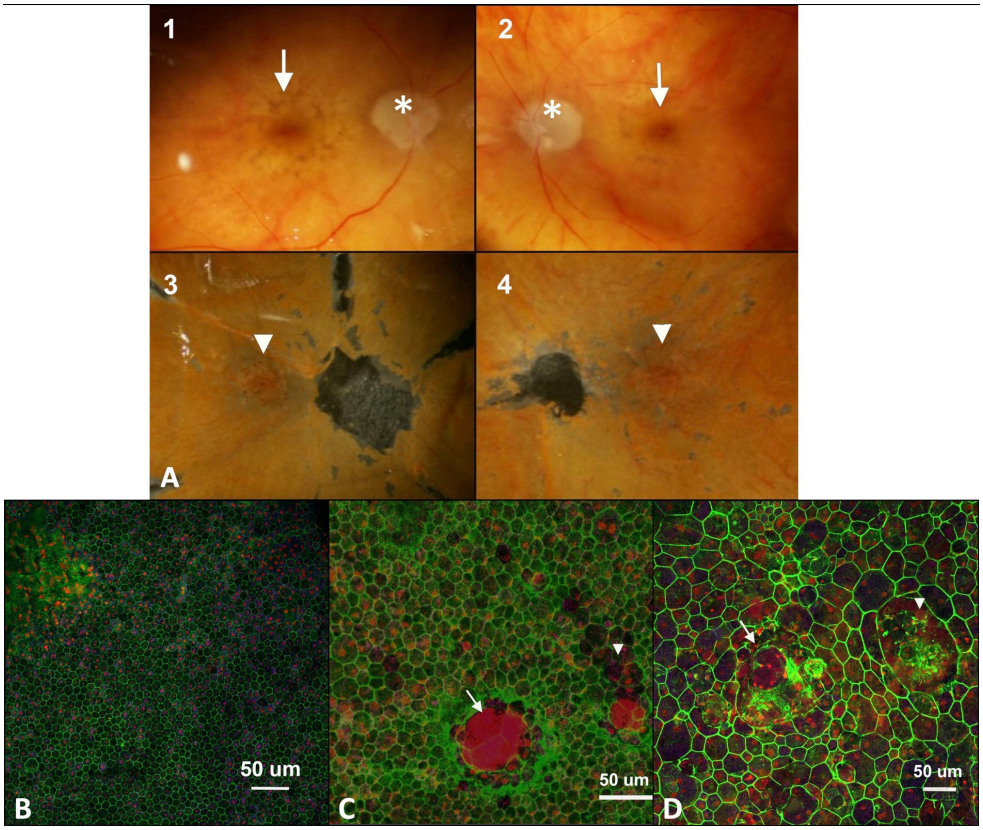


Figure 2. Representative images of retinal pigment epithelium (RPE) flatmounts. **A**1,2: Gross inspection of the posterior preparation of eyes in patient 1 with age-related macular degeneration (AMD) showed pigment mottling and drusen (arrows) within the macular area; optic nerve (asterix). **A**3,4: The RPE/Bruch's membrane/choroid preparations with preservation of the pigment mottling and drusen (arrowhead). **B**: RPE flatmount preparation showed normal RPE changes due to aging from a donor without AMD. **C**: RPE flatmount preparation showed drusen (arrow) and RPE atrophy (arrowhead) in right eye of patient 1 with AMD. **D**: RPE flatmount preparation showed drusen (arrow) and RPE atrophy (arrowhead) in left eye of patient 1 with AMD. The reconstructed surface area measured about 4 x 4 mm. (Panels **C** and **D**, RPE border is green, nucleus is red).

basal laminar deposit (BlamD) (Figure 3M-P). RPE cells were attenuated and degenerated overlying the drusen and BlamD. In the areas of small drusen <63 µm, there was a purse-string or rosette-like configuration of the overlying RPE; with medium size drusen 63-124 µm, the RPE cells were attenuated and thinly stretched over the surfaces of drusen; with large drusen ≥125 µm, surrounding neighboring RPE cells were deformed, and there were large, multinucleated RPE cells with irregular borders overlying the large drusen. Thick BlamD was present underlying continuous sheets of RPE cells. Bruch's membrane was thickened compared to the age matched control eyes and macrophages were present in the areas of thickened Bruch's membrane in the two AMD eyes that were examined by TEM. In a case of geographic atrophy, RPE cells overlying drusen were attenuated and depigmented in the area of geographic atrophy. The larger the drusen, the greater the likelihood that the surrounding RPE cells were disrupted or absent. Edges of zones of geographic atrophy were associated with a thick basal laminar deposit (BlamD). These findings were the only ones topographically localized in the 2D reconstruction and co-mapped one-to-one with the confocal images of RPE-choroid flatmount sheet.

Electron microscopic examination showed that in AMD eyes, Bruch's membrane was thickened and calcified (Figure

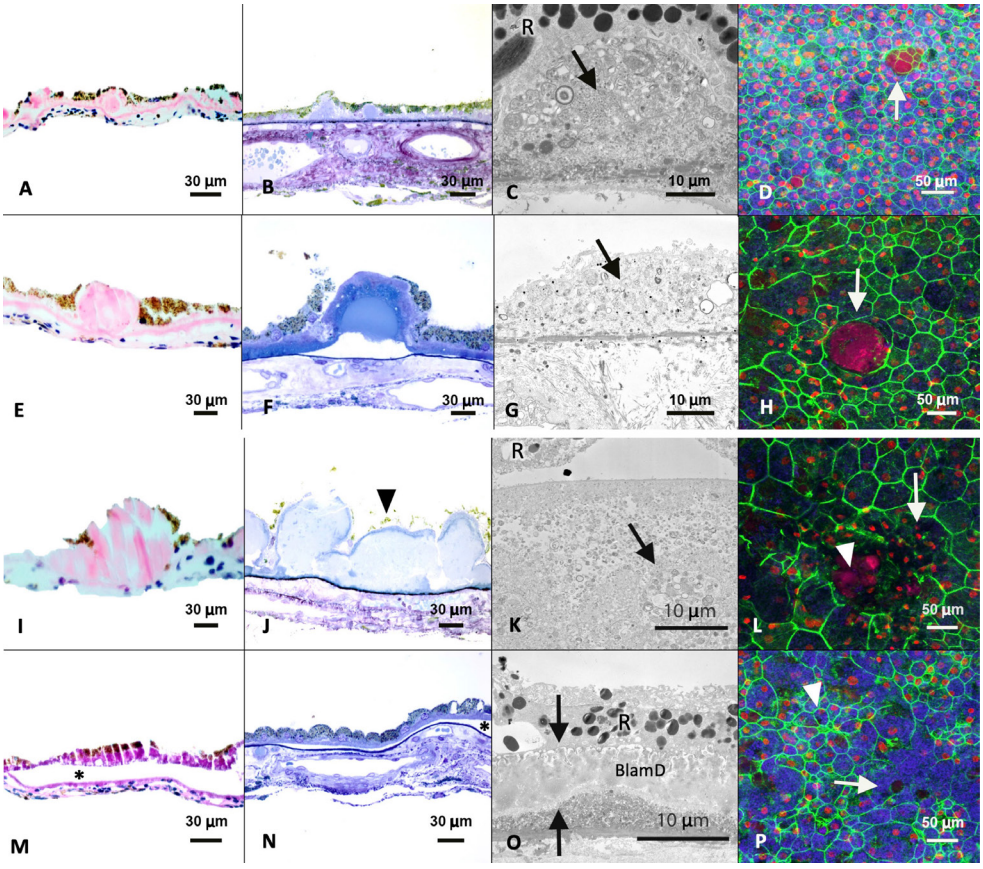


Figure 3. Drusen types, basal laminar deposit (BlamD), and corresponding retinal pigment epithelium (RPE) morphology. A-D. Small drusen (<63 µm). **A** and **B**: Small drusen are present between the RPE (arrowhead) and Bruch's membrane (arrow). **C**: The drusen are ultrastructurally composed of heterogeneous, variable electron-dense material (arrow). The RPE (R) overlying the drusen is intact (5,800X). **D**: The corresponding RPE flatmount shows a rosette overlying the small drusen (arrow) autofluorescence are shown in blue. **E-H**: Intermediate drusen (63-124 µm). **E** and **F**: The drusen form mounds between the RPE (arrowhead) basal lamina and inner collagenous layer of the Bruch's membrane (arrow); choroid (**C**). There is RPE loss overlying the apex of the druse. G. Intermediate druse is composed of heterogeneous electron dense material (arrow), which was not covered by RPE (4,800X). H. The corresponding RPE flatmount shows an irregular RPE surrounding the druse and RPE loss overlying the druse (arrow). **I-L**: Large drusen. **I** and **J**: The RPE overlying the large drusen shows loss of apical cytoplasm; the basal cytoplasm remains (arrowhead; 100X); choroid (C); Bruch's membrane (arrow), **K**: The drusen are ultrastructurally composed of more homogenous material (arrow) than small and intermediate drusen. The basal cytoplasm of the RPE (R) overlying the drusen is intact (5800X). **L**: The corresponding RPE flatmount loss of RPE cell borders and apparent fusion of RPE (green) with multiple nuclei (red; arrows) adjacent to the large druse (arrowhead). **M-P**: Basal laminar deposit (BlamD). **M** and **N**: The RPE/BlamD complex is detached (*) from the underlying Bruch's membrane and choroid. The RPE is intact. **O**: The BlamD (between arrows) is interposed between the plasma membrane and basal lamina of the RPE; choroid (C); RPE (arrowhead); Bruch's membrane (arrow) (5,800X) **P**: The corresponding RPE (green), including rosette formation (arrowhead), marked changes in cell size and shape, and RPE loss in areas (arrow). **E**,**I** (hematoxylin, high power objective [HPO]) M (periodic acid-Schiff, HPO), **B**, **F**, **J**, **N** (toluidine blue, HPO), **C** and **K** (osmium tetroxide/lead citrate, 5,800X), **G** and **O** (osmium tetroxide/lead citrate, 4,800X), **D**, **H**, **L**, **P** (AF635-phalloidin/propidium iodide 100X) RPE are green, druse and nucleus are red and autofluorescence are blue.

3O). BlamD, containing banded wide-spaced collagen and patches of electron-dense fibrillar or granular material, was present between the plasma membrane and the basement membrane of the RPE and internal to Bruch's membrane, was seen in all cases. The BlamD was distributed throughout the whole globe, including the macula and the periphery. Diffuse and amorphous BlamD was present within the inner collagenous zone of Bruch's membrane and was observed with coated and non-coated vesicles and membranous debris. In both aged normal eyes and AMD eyes, small, nodular drusen external to the RPE basal lamina were detected, sometimes contiguous with BlamD (Figure 3). Additionally, intermediate and large drusen were present external to the RPE basal lamina and contained amorphous material. (Figure 3G)

## DISCUSSION

In our study, we utilized the flatmount technique to investigate the relationship between RPE morphology and drusen/BlamD in human AMD eyes obtained post-mortem. We compared these en face versus cross-section findings while comparing age-matched control human eyes to AMD eyes. In the flatmount RPE-choroid sheet, we observed objects tentatively identified as large and diffuse soft drusen, irregularly shaped RPE with multiple nuclei, and areas with RPE defects in the macular region of the AMD eyes. In some areas, rosette-like structures were present, which we interpreted as representing the redistribution of RPE cells to fill in a potential gap surrounded by neighboring RPE cells. With the flatmount tissue preparation, cell area, variability in cell size, disruptions of cell form, and changes in the number of neighbors of RPE in AMD eyes may be further quantified with software such as Cellprofiler [14] and SpatStat [15]. (See [12,13,16,17] for application to RPE sheet analysis.)

Although the cellular patterns and mechanisms underlying RPE cell death in AMD remain unclear, it has been described previously that the impairment of RPE cell function is an early and crucial event in the molecular pathways leading to AMD [18,19]. One of the possible driving forces of the RPE dysfunction is an age-dependent phagocytic degeneration and metabolic insufficiency of RPE cells. This leads to reduced cellular capacity to degrade photoreceptor outer segments (POS) or cytoplasmic proteins in lysosomes and a progressive accumulation of intracellular lysosomal lipofuscin, which is composed mostly of lipids and proteins that are modified by chronic oxidative stress and inflammation [9,20-25]. Lipofuscin is a photoinducible generator of reactive oxygen species (ROS) that disturbs lysosomal integrity, induces lipid peroxidation, reduces phagocytic capacity, damages proteins and DNA, and finally may cause RPE cell death [19,26]. Moreover, impaired lysosomal degradation results in a significant reduction in autophagy, another clearance mechanism in RPE cells [21,27-29]. In our study, we observed aggregation of lipofuscin to varying degrees in AMD as intracellular autofluorescent deposits (pseudo colored in blue) in RPE flatmounts as reported in previous studies [30-33]. A schematic representation of the proposed mechanism on RPE loss and repair is shown in (Figure 4).

Drusen are deposited between the RPE and the inner collagenous zone of Bruch's membrane. Drusenogenesis is a complex and multifactorial process that takes place over many years. Lipids account for >40% of the volume in hard druse and probably a higher percentage in soft drusen [10,34]. We observed physical displacement and attenuation of the RPE monolayer overlying and adjacent to drusen in our study. RPE overlying drusen have altered autofluorescence (Figure 4), suggesting changes in RPE metabolism. Drusen may displace photoreceptors with concomitant changes in RPE architecture and function thus leading to cell death and eventual visual loss [29,35-42]. The presence of macular drusen correlates with abnormal contrast sensitivity in the central visual field [43,44]. Drusen formation is associated with the activation of the immune system and local inflammation. Proteomic and immunohistochemical analysis of drusen have revealed many protein constituents, including a number of immune-associated elements/molecules, immunoglobulins, class II antigens, and components of the complement cascade, activators, inhibitors (notably complement factor H, CFH), and terminal pathway components [45-49]. Activation of the complement system is a key component in drusenogenesis, RPE/photoreceptor degeneration, and Bruch's membrane disruption in AMD.

In the present study, we were able to identify histologic features of the lesions topographically located in the flatmount images and to propose mechanisms of RPE cell death in association with hard and soft drusen of small, medium and large sizes, and basal laminar deposit (BlamD). We propose mechanisms of RPE death as shown in (Figure 4A-D). In the death of a single RPE cell with small drusen (Figure 4A), we presume that the cell is extruded, and its immediate neighbors close around the central defect from the extruded RPE cell in a purse-string fashion, thus resulting in a rosette-like configuration. In the case of medium sized drusen (Figure 4B), we propose that small clusters of RPE die overlying the druse, and the adjacent RPE cells become attenuated and thinly stretched over the surfaces of druse. In the case of large drusen (Figure 4C), we propose that a small sheet of RPE exhibits necroptosis and is sloughed off the surface of the druse; some surrounding RPE either fuse and form large,

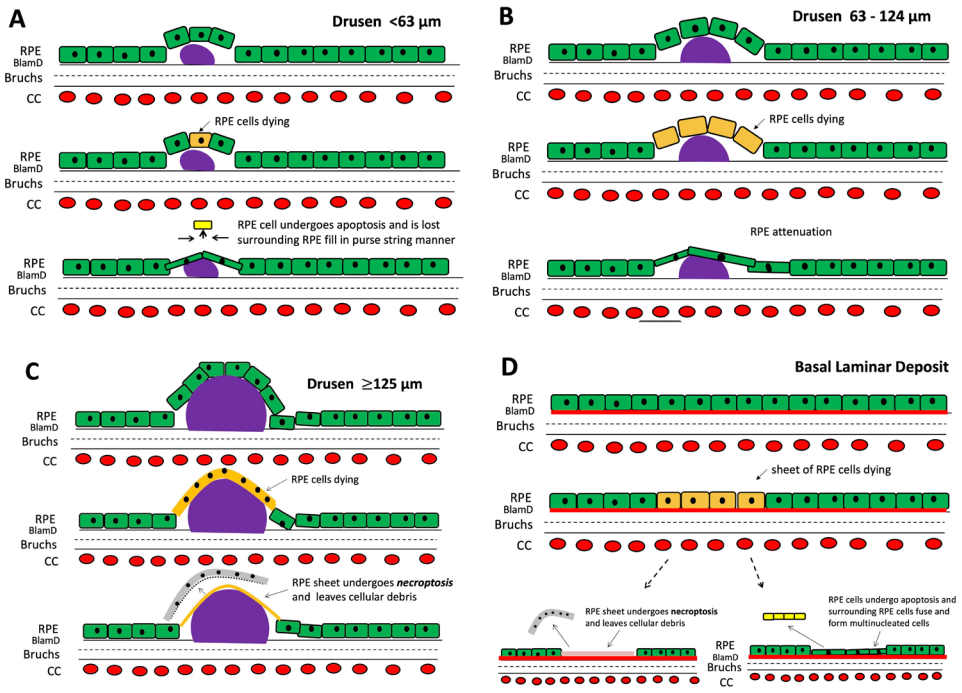


Figure 4. Schematic representation of retinal pigment epithelium (RPE) loss and repair. **A**: Small druse (<63 µm). The RPE pattern of a rosette filling in a defect is consistent with apoptosis of a single RPE cell overlying the small druse. **B**: Intermediate drusen (63-124 µm). The RPE pattern of complete loss overlying the intermediate druse is consistent with an autophagy mechanism of RPE cell loss. **C**: Large drusen (≥125 µm). The pattern of RPE loss with remaining basal cytoplasm overlying large drusen is consistent with necroptosis as a mechanism. **D**: Basal laminar deposit. RPE loss in sheets with preservation of basal cytoplasm and later multi-nucleated RPE is consistent with necroptosis, cell migration, and fusion as a mechanism of repair.

multinucleated cells or some exhibit nuclear division without cellular division, thus resulting in large, multinucleated cells overlying the large druse. In the case of geographic atrophy without drusen, the RPE may exhibit necroptosis or apoptosis with a resultant bare area of BlamD and migration of surrounding RPE that may overlie the BlamD (Figure 4D). Optical coherence tomography (OCT) data from previous study supports anterior cell migration [39]. In this study we are proposing that aside from RPE migration, necroptosis could be another mechanism. The weakness in our study is that it only descriptively compares the topographic pattern of human RPE cells in AMD eyes between the macula and the periphery and not quantitatively. Our future direction is to quantify the findings in this study and to perform further experiments to determine if the proposed mechanism results in the RPE pattern that we are seeing in this study.

In conclusion, we qualitatively evaluated eyes with AMD by microdissection of RPE flatmounts, and we compared that image to histological serial cross-sections cut perpendicular to the plane of the flatmount from the same RPE-choroid sheet. Mapping and co-registration of the two images was relatively easy by manual inspection. By registration of the en face RPE-choroid sheet image with the reconstructed image from histological cross-sections, we observed RPE rosette-like configurations overlying small drusen, attenuated/irregular RPE overlying medium size drusen, and large/multinucleated RPE cells overlying large drusen including soft drusen. In areas of geographic atrophy, we observed both absence of RPE and presence of irregularly shaped RPE overlying BlamD (Figure 3O,P). Several models of RPE cell death exist, and that they may be concurrent or sequential here we propose various mechanisms of RPE cell death and migration, which may result in these observed patterns (Figure 4A-D).

## ACKNOWLEDGMENTS:

This work was supported in part by the National Eye Institute R01EY028450, R01EY021592, P30EY006360, T32EY007092, F31EY028855, an unrestricted departmental grant from Research to Prevent Blindness, Inc., and an Emory Neuroscience Initiative Interdisciplinary Seed Grant.

## REFERENCES:

1. Klein R, Klein BEK, Jensen SC, Meuer SM. The five-year incidence and progression of age-related maculopathy: the Beaver Dam eye study. Ophthalmology 1997; 104:7-21. [PMID: 9022098].

2. Rudnicka AR, Kapetanakis VV, Jarrar Z, Wathern AK, Wormald R, Fletcher AE, Cook DG, Owen CG. Incidence of late-stage age-related macular degeneration in American whites: systematic review and meta-analysis. Am J Ophthalmol 2015; 160:85-93. [PMID: 25857680].

3. Algvere PV, Kvanta A, Seregard S. Drusen maculopathy: a risk factor for visual deterioration. Acta Ophthalmol 2016; 94:427-33. [PMID: 27009526].

4. Ambati J, Ambati BK, Yoo SH, Ianchulev S, Adamis AP. Age-related macular degeneration: etiology, pathogenesis, and therapeutic strategies. Surv Ophthalmol 2003; 48:257-93. [PMID: 12745003].

5. Winkler BS, Boulton ME, Gottsch JD, Sternberg P. Oxidative damage and age-related macular degeneration. Mol Vis 1999; 5:24-35. [PMID: 10562656].

6. Strauss O. The retinal pigment epithelium in visual function. Physiol Rev 2005; 85:845-81. [PMID: 15987797].

7. Okubo A, Rosa RH Jr, Bunce CV, Alexander RA, Fan JT, Bird AC, Luthert PJ. The relationships of age changes in retinal pigment epithelium and Bruch's membrane. Invest Ophthalmol Vis Sci 1999; 40:443-9. [PMID: 9950604].

8. Wing GL, Blanchard GC, Weiter JJ. The topography and age relationship of lipofuscin concentration in the retinal pigment epithelium. Invest Ophthalmol Vis Sci 1978; 17:601-7. [PMID: 669891].

9. Kinnunen K, Petrovski G, Moe MC, Berta A, Kaarniranta K. Molecular mechanisms of retinal pigment epithelium damage and development of age-related macular degeneration. Acta Ophthalmol 2012; 90:299-309. [PMID: 22112056].

10. Young RW. Pathophysiology of age-related macular degeneration. Surv Ophthalmol 1987; 31:291-306. [PMID: 3299827].

11. Alexander P, Thomson HA, Luff AJ, Lotery AJ. Retinal pigment epithelium transplantation: concepts, challenges, and future prospects. Eye (Lond) 2015; 29:992-1002. [PMID: 26043704].

12. Bhatia SK, Rashid A, Chrenek MA, Zhang Q, Bruce BB, Klein M, Boatright JH, Jiang Y, Grossniklaus HE, Nickerson JM. Analysis of RPE morphometry in human eyes. Mol Vis 2016; 22:898-916. [PMID: 27555739].

13. Boatright JH, Dalal N, Chrenek MA, Gardner C, Ziesel A, Jiang Y, Grossniklaus HE, Nickerson JM. Methodologies for analysis of patterning in the mouse RPE sheet. Mol Vis 2015; 21:40-60. [PMID: 25593512].

14. Lamprecht MR, Sabatini DM, Carpenter AE. CellProfiler(TM): free, versatile software for automated biological image analysis. Biotechniques 2007; 42:71-5. [PMID: 17269487].

15. Baddeley A, Turner R. spatstat: An R package for analyzing spatial point patterns. J Stat Softw 2005; 12:1-42. http://www.spatstat.org/resources/spatstatJSSpaper.pdf.

16. Rashid A, Bhatia SK, Mazzitello KI, Chrenek MA, Zhang Q, Boatright JH, Grossniklaus HE, Jiang Y, Nickerson JM. RPE Cell and sheet properties in normal and diseased eyes. Adv Exp Med Biol 2016; 854:757-63. [PMID: 26427486].

17. Jiang Y, Qi X, Chrenek MA, Gardner C, Boatright JH, Grossniklaus HE, Nickerson JM. Functional principal component analysis reveals discriminating categories of retinal pigment epithelial morphology in mice. Invest Ophthalmol Vis Sci 2013; 54:7274-83. [PMID: 24114543].

18. Kay P, Yang YC, Paraoan L. Directional protein secretion by the retinal pigment epithelium: roles in retinal health and the development of age-related macular degeneration. J Cell Mol Med 2013; 17:833-43. [PMID: 23663427].

19. Kopitz J, Holz FG, Kaemmerer E, Schutt F. Lipids and lipid peroxidation products in the pathogenesis of age-related macular degeneration. Biochimie 2004; 86:825-31. [PMID: 15589692].

20. Abdelsalam A, Del Priore L, Zarbin MA. Drusen in age-related macular degeneration: pathogenesis, natural course, and laser photocoagulation-induced regression. Surv Ophthalmol 1999; 44:1-29. [PMID: 10466585].

21. Karlsson M, Kurz T. Attenuation of iron-binding proteins in ARPE-19 cells reduces their resistance to oxidative stress. Acta Ophthalmologica. 2016; 94:556-64. [PMID: 27287874].

22. Brandstetter C, Holz FG, Krohne TU. Complement component C5a primes retinal pigment epithelial cells for inflammasome activation by lipofuscin-mediated photooxidative damage. J Biol Chem 2015; 290:31189-98. [PMID: 26565031].

23. Mohr LKM, Hoffmann AV, Brandstetter C, Holz FG, Krohne TU. Effects of inflammasome activation on secretion of inflammatory cytokines and vascular endothelial growth factor by retinal rigment epithelial cells. Invest Ophthalmol Vis Sci 2015; 56:6404-13. [PMID: 26444721].

24. Ferrington DA, Sinha D, Kaarniranta K. Defects in retinal pigment epithelial cell proteolysis and the pathology associated with age-related macular degeneration. Prog Retin Eye Res 2016; 51:69-89. [PMID: 26344735].

25. Nowak JZ. Oxidative stress, polyunsaturated fatty acids-derived oxidation products and bisretinoids as potential inducers of CNS diseases: focus on age-related macular degeneration. Pharmacol Rep 2013; 65:288-304. [PMID: 23744414].

26. Brunk UT, Terman A. Lipofuscin: mechanisms of age-related accumulation and influence on cell function. Free Radic Biol Med 2002; 33:611-9. [PMID: 12208347].

27. Sadigh S, Luo XD, Cideciyan AV, Sumaroka A, Boxley SL, Hall LM, Sheplock R, Feuer WJ, Stambolian DS, Jacobson SG. Drusen and photoreceptor abnormalities in African-Americans with intermediate non-neovascular age-related macular degeneration. Curr Eye Res 2015; 40:398-406. [PMID: 24912073].

28. Blasiak J, Petrovski G, Vereb Z, Facsko A, Kaarniranta K. Oxidative stress, hypoxia, and autophagy in the neovascular processes of age-related macular degeneration. BioMed Res Int 2014; 2014:768026-[PMID: 24707498].

29. Sadigh S, Cideciyan AV, Sumaroka A, Huang WC, Luo XD, Swider M, Steinberg JD, Stambolian D, Jacobson SG. Abnormal thickening as well as thinning of the photoreceptor layer in intermediate age-related macular degeneration. Invest Ophthalmol Vis Sci 2013; 54:1603-12. [PMID: 23361506].

30. Ach T, Tolstik E, Messinger JD, Zarubina AV, Heintzmann R, Curcio CA. Lipofuscin redistribution and loss accompanied

by cytoskeletal stress in retinal pigment epithelium of eyes with age-related macular degeneration. Invest Ophthalmol Vis Sci 2015; 56:3242-52. [PMID: 25758814].

31. Ding JD, Johnson LV, Herrmann R, Farsiu S, Smith SG, Groelle M, Mace BE, Sullivan P, Jamison JA, Kelly U, Harrabi O, Bollini SS, Dilley J, Kobayashi D, Kuang B, Li W, Pons J, Lin JC, Bowes Rickman C. Anti-amyloid therapy protects against retinal pigmented epithelium damage and vision loss in a model of age-related macular degeneration. Proc Natl Acad Sci USA 2011; 108:E279-87. [PMID: 21690377].
32. Rudolf M, Vogt SD, Curcio CA, Huisingh C, McGwin G Jr, Wagner A, Grisanti S, Read RW. Histologic basis of variations in retinal pigment epithelium autofluorescence in eyes with geographic atrophy. Ophthalmology 2013; 120:821-8. [PMID: 23357621].
33. Zanzottera EC, Ach T, Huisingh C, Messinger JD, Freund KB, Curcio CA. visualizing retinal pigment epithelium phenotypes in the transition to atrophy in neovascular age-related macular degeneration. Retina 2016; 36:Suppl 1S26-39. [PMID: 28005661].
34. Green WR. Histopathology of age-related macular degeneration. Mol Vis 1999; 5:27-[PMID: 10562651].
35. Dorey CK, Wu G, Ebenstein D, Garsd A, Weiter JJ. Cell loss in the aging retina. relationship to lipofuscin accumulation and macular degeneration. Invest Ophthalmol Vis Sci 1989; 30:1691-9. [PMID: 2759786].
36. Theodossiadis PG, Theodoropoulou S, Stamatiou P, Datseris I, Theodossiadis GP. Photoreceptor layer changes overlying drusen in eyes with age-related macular degeneration associated with vitreomacular traction. Eur J Ophthalmol 2014; 24:582-92. [PMID: 24338584].
37. Mrejen S, Sato T, Curcio CA, Spaide RF. Assessing the cone photoreceptor mosaic in eyes with pseudodrusen and soft drusen in vivo using adaptive optics imaging. Ophthalmology 2014; 121:545-51. [PMID: 24183341].
38. Spaide RF. Outer retinal atrophy after regression of subretinal drusenoid deposits as a newly recognized form of late age-related macular degeneration. Retina-J Ret Vit Dis. 2013; 33:1800-8. [PMID: 23764969].
39. Curcio CA, Messinger JD, Sloan KR, McGwin G, Medeiros NE, Spaide RF. Subretinal drusenoid deposits in non-neovascular age-related macular degeneration: morphology, prevalence, topography, and biogenesis model. Retina 2013; 33:265-76. [PMID: 23266879].
40. Mettu PS, Wielgus AR, Ong SS, Cousins SW. Retinal pigment epithelium response to oxidant injury in the pathogenesis of early age-related macular degeneration. Mol Aspects Med 2012; 33:376-98. [PMID: 22575354].
41. Zarbin MA. Current concepts in the pathogenesis of age-related macular degeneration. Arch Ophthalmol-Chic. 2004; 122:598-614. [PMID: 15078679].
42. Adler R, Curcio C, Hicks D, Price D, Wong F. Cell death in age-related macular degeneration. Mol Vis 1999; 5:31-[PMID: 10562655].
43. Mitrut I, Verma A, Madill S, Smith RT, Chong NV. Color contrast and drusen area. Ophthalmology 2010; 117:1280-1. [PMID: 20522345].
44. Roh M, Selivanova A, Shin HJ, Miller JW, Jackson ML. Visual acuity and contrast sensitivity are two important factors affecting vision-related quality of life in advanced age-related macular degeneration. PLoS One 2018; 13:e0196481-[PMID: 29746512].
45. Campagne MV, Strauss EC, Yaspan BL. Age-related macular degeneration: complement in action. Immunobiology 2016; 221:733-9. [PMID: 26742632].
46. Wagner EK, Raychaudhuri S, Villalonga MB, Java A, Triebwasser MP, Daly MJ, Atkinson JP, Seddon JM. Mapping rare, deleterious mutations in factor h: association with early onset, drusen burden, and lower antigenic levels in familial AMD. Sci Rep 2016; •••:6-[PMID: 27572114].
47. Hughes AE, Bridgett S, Meng WH, Li MY, Curcio CA, Stambolian D, Bradley DT. Sequence and expression of complement factor H gene cluster variants and their roles in age-related macular degeneration risk. Invest Ophthalmol Vis Sci 2016; 57:2763-9. [PMID: 27196323].
48. Kim HJ, Ahn SJ, Woo SJ, Hong HK, Suh EJ, Ahn J, Park JH, Ryoo NK, Lee JE, Kim KW, Park KH, Lee C. Proteomics-based identification and validation of novel plasma biomarkers phospholipid transfer protein and mannan-binding lectin serine protease-1 in age-related macular degeneration. Sci Rep-Uk. 2016;6.
49. Kim SY, Assawachananont J. A new method to visualize the intact subretina from retinal pigment epithelium to retinal tissue in whole mount of pigmented mouse eyes. Transl Vis Sci Technol 2016; 5:6-[PMID: 26929886].

Articles are provided courtesy of Emory University and the Zhongshan Ophthalmic Center, Sun Yat-sen University, P.R. China. The print version of this article was created on 7 February 2019. This reflects all typographical corrections and errata to the article through that date. Details of any changes may be found in the online version of the article.